Paper No.
19073

AMPP ANNUAL CONFERENCE + EXPO
MARCH 19-23, 2023 | DENVER, COLORADO

Kinetics of Iron Dissolution: A New Approach for Modeling the Anodic Potentiodynamics Based on Transient Analysis

Mohiedin Bagheri Hariri, Bruce Brown, and Srdjan Nesic

Institute for Corrosion and Multiphase Technology
Department of Chemical & Biomolecular Engineering
Ohio University
342 West State Street
Athens, Ohio, 45701
USA

ABSTRACT

In this work, a new approach is introduced to determine the kinetic constants of the elementary steps involved in the overall reaction of iron anodic dissolution. A procedure based on transient analysis is established, for the first time, that enables the estimation of a series of kinetic parameters that can be used for modeling the anodic potentiodynamics over a wide range of environmental conditions. The findings of the present research enhance the ability of explaining how different environmental factors (CO_2 presence, pH, temperature, steel type, etc.) mechanistically affect the kinetics of iron dissolution.

INTRODUCTION

Although extensive research has been carried out on modeling the cathodic potentiodynamic sweep during the corrosion of iron/steel, previous studies have not been able to layout a systematic approach to mechanistically describe the kinetics and model anodic dissolution. This study offers some insights into the mechanistic modeling of electrochemical anodic reactions at different experimental conditions. For iron dissolution, there are two well-known mechanisms valid for strong acid solutions (pH ≤ 4) in the literature; namely, the “catalytic mechanism” proposed by Heusler et al.,[1] and the “consecutive mechanism” proposed by Bockris et al.[2] In 1981 and 1986, Keddam, et al.,[4-7] reported that multiple dissolution paths exist as several time constants were observed during EIS measurements under well controlled experimental conditions. They claimed that more than one single intermediate and three dissolution paths can be occurring in parallel during iron dissolution under certain experimental

conditions. Hence, Keddam, et al., combined both consecutive and catalytic mechanisms into a single multipath scheme (Figure 1) to define a plausible explanation for such observations.[4]

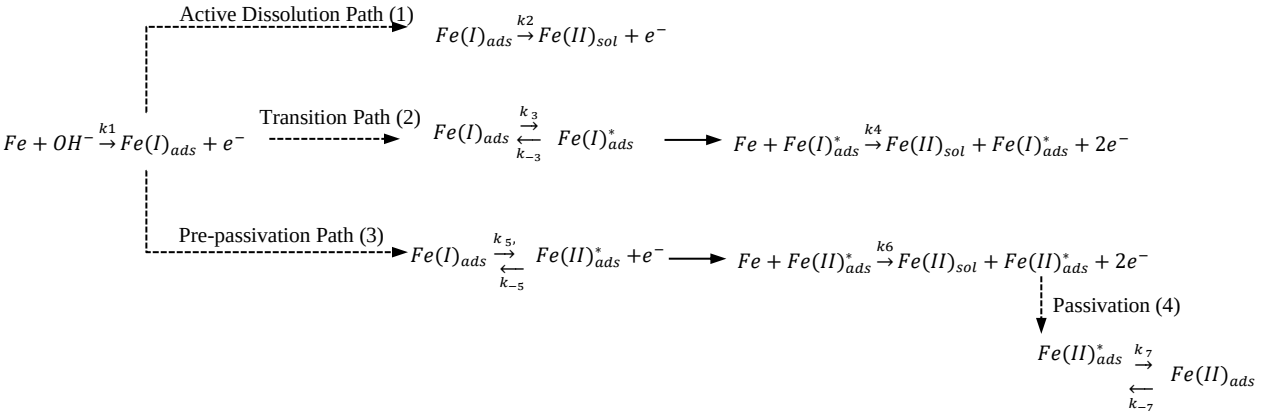

Figure 1. The multipath iron dissolution mechanism, adapted from Keddam et al.[4]

In this scheme (Figure 1), the first and the second elementary steps (Path (1)) approximate the Bockris' mechanism (non-catalytic path).[2] In our previous research,[8] thirty-eight different pathways were investigated for the mechanism of iron dissolution in strong acid and it was found that the experimental observations in the active range of dissolution were explainable only by relying on Bockris' mechanism.[2]

Figure 2 shows an anodic sweep for a pure iron rotating disk electrode (RDE) sample in 0.5 M Na_2SO_4 electrolyte at pH 5 (25 °C). In Figure 2, at low anodic overpotentials, active dissolution takes place, while a decrease in current density can be observed at more positive overpotentials in the transition range. This behavior is described as the "S-shape" segment of the anodic sweep. At more positive overpotentials beyond the transition region, there is an increase in current which is defined as the pre-passivation dissolution range, followed by the passive state and a marked drop in the current density. These transformations in the anodic sweep cannot be explained by assuming only a single dissolution path (or a single adsorbed intermediate) as hypothesized by Bockris.[2]

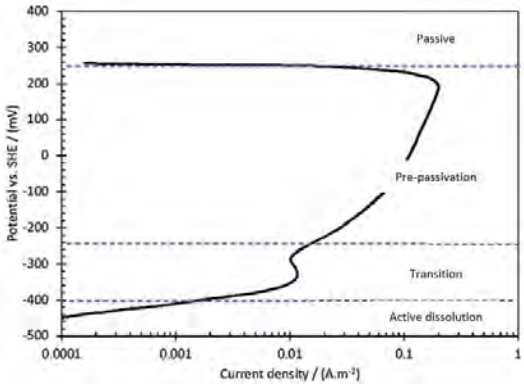

Figure 2. Anodic sweep for pure iron RDE sample in 0.5M Na_2SO_4 at pH 5 (25 °C), scan rate: 6.6 mV/s, rotation rate: 4140 rpm.[3]

At more positive overpotentials, paths (2) and (3) are written following Heusler's catalytic iron dissolution mechanism.[1] The reason they are called catalytic is because of the formation of an intermediate (those compounds marked by a star) that can react more readily with another reactant to proceed with the dissolution reaction much faster. These intermediates are neither consumed nor produced.

Although it seems comprehensive, Keddam's multipath scheme[4] is very complex. Seven elementary steps with 20 kinetic constants make it almost impossible to determine independent values

for each of them using a methodical approach. Keddam et al.[4] used trial and error to determine the various kinetic constants in order to model the entire potentiodynamic sweep range as well as EIS data. In contrast, a different approach is developed in the present study to estimate the kinetic parameters using a simplified theory. In order to do that, the scheme developed by Keddam et al.[4] needed to be abridged to have fewer degrees of freedom, enabling the introduction of a deterministic method for estimating the parameters and subsequently modeling the anodic sweeps.

A two-path scheme, shown in Figure 3, is proposed in this study. In this scheme, the non-catalytic path is in parallel with only one catalytic path. Indeed, this idea combines two fundamental theories into a single one without any further complications. In this work, it has been proposed that using this scheme can reasonably model the anodic potentiodynamic and capture the nonlinearity of the anodic sweep over the potential ranges slightly above the transition region as shown in Figure 4. This simplified scheme is more pragmatic since it provides a platform based on which one can more easily model the steady-state kinetics. In addition, this platform enhances the capability of describing the influence of different environmental/metallurgical factors on anodic dissolution.

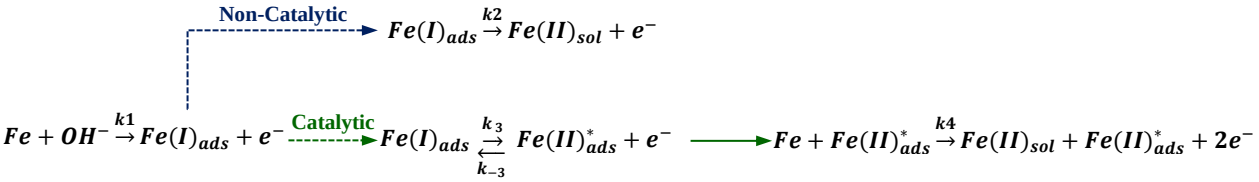

Figure 3. The theoretical scheme introduced in this study.

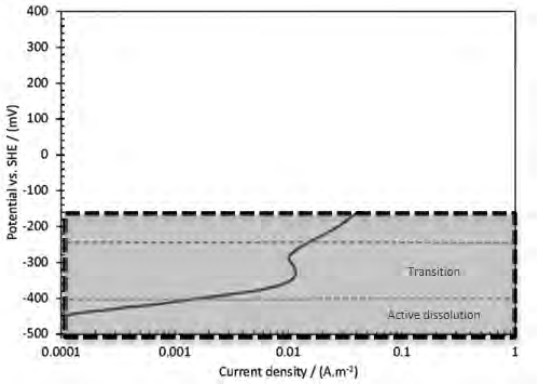

Figure 4. The range of interest for the current corrosion studies.

A few assumptions have been made in this study. First, it has been assumed that no corrosion product is produced. Although the applicability of the present work for corrosion modeling is promising, the formation of corrosion film adds further complexities beyond the scope of the present work. It is also assumed that the reaction rate for each elementary step (i) follows an exponential function of potential as described by Eq. 1 (Tafel law):

$$k_i = k_{i,0} \exp\left(2.3E/b_i\right) \quad (1)$$

where $k_{0,i}$ is k_i at the reference potential of zero vs. SHE reference electrode. b_i is the Tafel value or the magnitude of the polarization that is needed to initiate that specific elementary step. k_i is a function

of potential. The kinetic parameters $k_{0,i}$, and b_i are independent of potential but are influenced by environmental parameters such as pH, temperature, electrolyte, etc. b_i is different from the conventional known Tafel slope, as the latter one is defined for only the overall reaction containing a single rate-determining step (rds). Considering the new scheme shown in Figure 3, there are five potential-dependant k_i and each one contains two potential-independent variables ($k_{0,i}$, and b_i). Therefore, ten kinetic parameters need to be estimated in this study for every experimental condition ($k_{0,1}$, $k_{0,2}$, $k_{0,3}$, $k_{0,-3}$, $k_{0,4}$, b_1, b_2, b_3, b_{-3}, b_4; where b_i is in V/dec. and $k_{0,i}$ is in mol.m^{-2}.s^{-1}).

EXPERIMENTAL METHOD

A 2-liter glass cell with a rotating cylinder electrode (RCE) as a working electrode (WE) was used. A ring-shaped platinum-coated titanium mesh counter electrode (CE) was used for completing the circuit to allow the charge to flow, and an Ag/AgCl reference electrode (RE) was used with respect to which all potentials were measured. The ring-shaped counter electrode was used to provide a more symmetric current distribution around the rotating WE. An overview of the experimental setup and test matrix are shown in Figure 5.

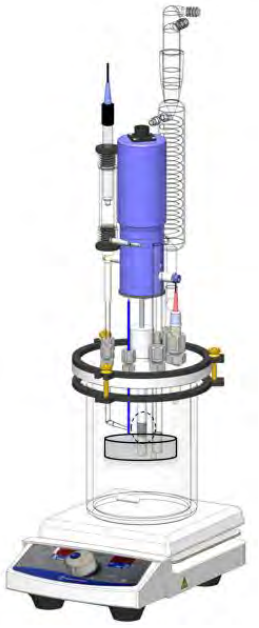

Parameter	Conditions
pH (±0.02)	4 - 6
Environment	Strong acid: 0.97 bar N_2 sparged
	Weak acid: 0.97 bar CO_2 sparged
Electrolyte	2.5 – 2.9 wt.% NaCl (R_s ~ 0.78±0.08 Ω for all measurements)
rpm	100, 1000
Temp. (±0.5) °C	25 - 45
Test set-up	2L glass cell, RCE
Motor rotation speed	2000 rpm
Materials	Pure Fe, X65, 2% Cr steel

Figure 5. Overview of the RCE experimental setup and test matrix.

Potentiodynamic and potentiostatic transient measurements with a high sampling rate (~3 microseconds per data point) were conducted using a Gamry potentiostat Reference 600. Each test was repeated at least four times to reduce the statistical uncertainty. Uncertainty for all measurements is reported in this study. All RCE specimens were polished up to 1200-grit, rinsed with DI water and isopropanol alcohol, and dried with nitrogen gas before every experiment. High-purity N_2 or CO_2 gas was sparged continuously through the test solution to de-oxygenate the electrolyte during all measurements. Diluted NaOH and HCl were used to adjust the pH. It was important to make sure that the solution resistance for all measurements was the same. Before each measurement, EIS was recorded to assure that the solution resistance was consistent for all measurements and always within the range of 0.78 ±0.08 Ω.

RESULTS & DISCUSSION

Summary of the Proposed Approach

Steady-state and transient measurements were used in parallel to determine the kinetic constants of the elementary steps. The main challenge was exploring a mechanistic approach using transient analysis based on a simplified theory, to calculate the kinetic constants (Figure 3) for iron anodic dissolution. As mentioned above, there are 10 kinetic parameters for each environmental condition that needed to be obtained. Steady-state and transient measurements were used in parallel to determine the constants. Figure 6 represents the general steps and the range of data points that were used to calculate a particular kinetic parameter(s). The first step was to collect repeatable anodic potentiodynamic sweeps and specify the appropriate potential range of active, transition, or pre-passivation domains to be used in subsequent potential perturbations. The blue highlighted areas in Figure 6 (b) through (f) illustrate the range of data used to approximate k_1, k_2, k_3, k_4, and k_{-3}, respectively at a given fixed potential.

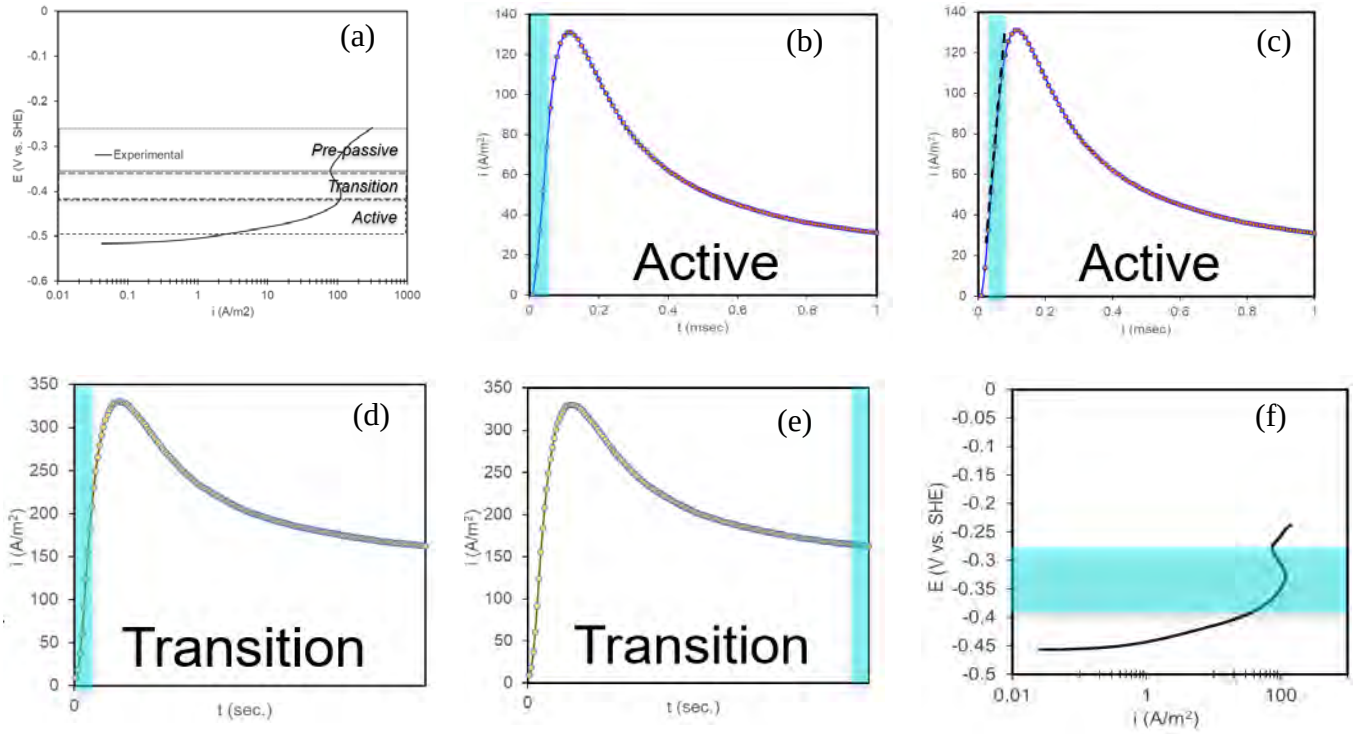

Figure 6. (a) Specifying the appropriate range for potential perturbation, and the range of data points used to calculate the kinetic parameters (b) k_1, (c) k_2, (d) k_3, (e) k_4, and (f) k_{-3}.

Table 1 summarizes the electrochemical technique, methodology and the mathematical correlation used to estimate the corresponding constant. The brief theory behind these mathematical expressions and methodology to obtain k_i values will be explained.

Table 1. Summary of the proposed approach to estimate kinetic parameters of each elementary step

Parameter	Technique	Methodology	Approach for estimation
k_1	Potentiostatic	A set of transients in active domain	$i_{t=0^+} \approx Fk_1$
k_2	Potentiostatic	A set of transients in active domain	$\left.\frac{di}{dt}\right\|_{t=0^+} : k_2$
k_3	Potentiostatic	A set of transients in transition domain	$i_{t=0^+} \approx 2Fk_3^*$
k_4	Sampled steady-state	A set of transients in transition domain	$i_{st.st} \approx 2Fk_4$
k_{-3}	Potentiodynamic	A set of data points from anodic polarization	$k_{-3}(E) = A + Bk_4$

k_1 Estimation: At OCP, the iron surface is almost entirely covered with hydrogen. With a positive perturbation in the potential of the iron surface, hydrogen desorption is achievable, but only at high overpotentials (> 60 mV vs. OCP).[4] In the active domain, the non-catalytic path (Figure 3) is the dominant reaction pathway. By applying a positive potential perturbation, the electrons are "pulled out" of the WE leading to a quick "pile-up" of $Fe(I)_{ads}$ according to the first step. Let's assume that θ_1 is the fraction of the surface that is covered with chemisorbed non-catalytic $Fe(I)_{ads.}$ intermediate. Similarly, θ_2 is the fraction of the surface that is occupied by a chemisorbed catalytic $Fe(II)_{ads}^*$ intermediate. θ_i is a function of time and potential, but at a fixed potential it's only a function of time ($\theta_i(t)$). Writing the charge balance equation, "$1-\theta_1$" fraction of the surface is available for step 1 and "θ_1" fraction of the surface is available for step 2, hence the total current is given by:

$$\frac{i(t)}{F} = k_1(1-\theta_1(t)) + k_2\theta_1(t) \quad (2)$$

Before applying potential perturbation. the surface is completely covered by hydrogen and the surface coverage due to $Fe(I)_{ads}$ is almost negligible,[4], therefore, the initial coverage $\theta_1(t = 0) \approx 0$. Therefore, according to Eq. 2, the current response right after the potential perturbation at time $t = 0^+$ (~ at 6 microseconds) is approximately equal to Fk_1:

$$\frac{i(0^+)_{active}}{F} \approx k_1 \quad (3)$$

By plotting the natural logarithm of k_1 versus potential, the kinetic parameters for the first elementary ($k_{0,1}$ and b_1) were obtained.

k_2 Estimation: k_2 can be derived by writing a mass balance expression (Eq. 4) to describe the variation of θ_1 as a function of time. $Fe(I)_{ads}$ is produced in the first step and is consumed in the second step, thus:

$$\beta\frac{d\theta_1}{dt} = k_1(1-\theta_1) - k_2\theta_1 \quad (4)$$

where β is a constant, linking the fraction of the surface coverage, θ_1, and the surface concentration of the chemisorbed species. By solving the first order differential Eq. 4, $\theta_1(t)$ can be expressed according to:

$$\theta_1(t) = \left(\frac{k_1}{k_1+k_2}\right) \times \left\{1 - e^{-\left(\frac{k_1+k_2}{\beta}\right)t}\right\} \quad (5)$$

From Eqs. 4 and 5 one obtains:

$$\frac{d(i(t))}{dt} = \frac{Fd\theta_1}{dt}(k_2 - k_1) \quad (6)$$

$$\frac{d\theta_1(t)}{dt} = \left(\frac{k_1}{\beta}\right) \times e^{-\left(\frac{k_1+k_2}{\beta}\right)t} \quad (7)$$

Substituting Eq. 5 into Eq. 7, and taking the natural logarithm of both sides, one obtains:

$$ln\left(\frac{di(t)}{dt}\right) = ln\left(\frac{Fk_1(k_2-k_1)}{\beta}\right) - \left(\frac{k_1+k_2}{\beta}\right)t \quad (8)$$

Therefore, by plotting $ln\left(\frac{di(t)}{dt}\right)$ as a function of time (for the time interval slightly after t = 0^+ and before the peak current) at a fixed potential and given that k_1 was already determined, k_2 can be calculated at a constant potential. The dependence of k_2 on potential was defined according to an exponential function, thus b_2 and $k_{0,2}$ can be attained by plotting the natural logarithm of k_2 versus potential.

k_3 Estimation: In the transition range of a potential perturbation, the current is not only coming from the non-catalytic pathway but also from the catalytic path as shown in Figure 3. Therefore, when writing a charge balance equation for the transition range, both θ_1 and θ_2 are involved in the production of current according to:

$$\frac{i(t)}{F} = 2k_3^*(1-\theta_2) - 2k_{-3}^*\theta_2 + 2k_4\theta_2 + k_2\theta_1 \quad (9)$$

The net current in the potential ranges of the transition domain results from both step 1 and step 3. In this regard, the overall kinetics are under the control of steps 1 and 3. Therefore, the net rate is coming from these two steps 1 and 3. k_3^* is introduced as the harmonic average of both steps 1 and 3 and can be expressed as:

$$k_3^* = \left(\frac{1}{k_1} + \frac{1}{k_3}\right)^{-1} \quad (10)$$

Before applying potential perturbation, the surface is completely covered by hydrogen and the surface coverage due to $Fe(I)_{ads}$ and $Fe(II)_{ads}^*$ are almost negligible, therefore the initial coverage θ_1 and θ_2 at t = 0 is almost zero. Thus, according to Eq. 9, the current response right after the potential perturbation at time t = 0^+ (~ at 6 microseconds) is approximately equal to $2Fk_3^*$:

$$\frac{i(0^+)_{transition}}{F} \approx 2k_3^* \quad (11)$$

Having a set of transients at different potentials in the range of the transition domain, one can obtain k_3^* as a function of potential. Having k_3^* and given that $k_{0,1}$ and b_1 are already calculated, Eq. 12 can be used to obtain k_3 at different potentials:

$$k_3 = \left(\frac{1}{k_3^*} - \frac{1}{k_1}\right)^{-1} \quad (12)$$

By plotting the natural logarithm of k_3 versus potential, the kinetic parameters for step 3 ($k_{0,3}$ and b_3) can be estimated.

k_4 Estimation: k_4 was estimated using sampled steady-state data points which is the current response when the transients reach a plateau. Writing the charge balance equation from the scheme shown in Figure 3 we have:

$$\frac{i(t)}{F} = k_1(1-\theta_1-\theta_2) + (k_2+k_3)\theta_1 + (2k_4 - k_{-3})\theta_2 \quad (13)$$

From mass balance equation for the chemisorbed entities $Fe(I)_{ads}$ and $Fe(II)_{ads}^{*}$, the time-dependence of θ_1 and θ_2 can be obtained through the following differential equations:

$$\beta \frac{d\theta_1}{dt} = k_1(1-\theta_1-\theta_2) - (k_2+k_3)\theta_1 + k_{-3}\theta_2 \quad (14)$$

$$\beta \frac{d\theta_2}{dt} = k_3\theta_1 - k_{-3}\theta_2 \quad (15)$$

where at steady-state (*st.st*) the constant values for the surface coverages (θ_1 and θ_2) vs. time make the first derivative of θ_i vs. time equal to zero:

$$\frac{d\theta_1}{dt} = 0 \quad \Rightarrow \quad \theta_{1,st.st} = \frac{k_1 k_{-3}}{k_1k_3 + k_1k_{-3} + k_2k_{-3}} \quad (16)$$

$$\frac{d\theta_2}{dt} = 0 \quad \Rightarrow \theta_{2,st.st} = \frac{k_1 k_3}{k_1k_3 + k_1k_{-3} + k_2k_{-3}} \quad (17)$$

Putting $\theta_{i,st.st}$ into the Eq. 13, one can obtain the steady-state current density as:

$$i_{sampled\ st.st} = \frac{2Fk_1(k_2k_{-3}+k_4k_3)}{k_1k_3 + k_{-3}(k_1+k_2)} = 2Fk_2\theta_{1,stst} + 2Fk_4\theta_{2,stst} \quad (18)$$

By assuming that $k_{-3} \ll k_4$, Eq. 18 can be simplified to:

$$i_{sampled\ st.st} \approx 2Fk_4 \quad (19)$$

Thus, having a set of transients at different potentials in the range of the transition domain, one can obtain k_4 using sampled steady-state data. By plotting the natural logarithm of k_3 versus potential, the kinetic parameters for step 3 ($k_{0,3}$ and b_3) can be estimated.

k_{-3} Estimation: k_{-3} in the active range of potentials near transition, tends to push step 3 in the backward direction, resisting the imposed perturbation and reducing the net current. While, in the transition range, the current decreases at higher overpotentials. Therefore, the value of b_{-3} should be negative in the active domain and positive in the transition range of potential perturbation. An analytical approach was used to obtain k_{-3} using a set of data points taken from anodic potentiodynamics. From the steady-state equation, k_{-3} can be written as a function of k_4:

$$k_{-3}(E) = Bk_4 + A \quad (20)$$

where A and B are a function of potential and by rearranging Eq. 18, they can be expressed as:

$$A(E) = \frac{i_{st.st}k_1k_3}{2Fk_1k_2 - i_{st.st}(k_1+k_2)} \quad (21)$$

$$B(E) = \frac{-2Fk_1k_3}{2Fk_1k_2 - i_{st.st}(k_1+k_2)} \quad (22)$$

Using Eqs. (20-22), k_{-3} can be determined at different potentials. k_{-3} was presumably an exponential function of potential, $k_{0,-3,}$ and b_{-3} can be computed in the active and transition domains, separately using regression lines on a semi-logarithmic scale. For calculating k_{-3} in the transition region, similar steps were followed, and the net k_{-3} was estimated by superposing $k_{-3,active}$ + $k_{-3,transition}$. Table 2 summarizes the calculated kinetic parameters using the abovementioned transient approach for different experimental conditions. In this study, every measurement was repeated at least four times. Several kinetic parameters, k_i, are derived from experimental transients and applying the average value, $k_{,i,avg}$ (Table 2), in the model could reproduce the experimental potentiodynamics. Different algorithms were used to estimate the uncertainty associated with each computed parameter. It is essential to know the largest possible range of error so that in case of not having the best match, the range in which a particular parameter can be "tuned" would be known. Parameters that are marked with a star (*) were slightly tuned within the range of uncertainty for a better fit. The anodic potentiodynamics were modeled in this study by inserting these parameters into the equations above. In Table 2, b_i is presented in V/dec. and $k_{0,i}$ is in $mol.m^{-2}.s^{-1}$.

Table 2. Summary of the rate constants at different test conditions derived using the proposed transient methodology in this study

Condition	$k_{0,1}$	b_1	$k_{0,2}$	b_2	$k_{0,3}$	b_3	$k_{0,-3,act.}$	$b_{-3,act.}$	$k_{0,-3,trams.}$	$b_{-3,trans.}$	$k_{0,4}$	b_4
Fe, 25°C, pH4, N_2	4.9×10^{-2}*	0.12±0.02	1.57×10^{-1}	0.26±0.09	1.03×10^{-3}	0.34±0.1	1.3×10^{-20} *	-0.028*	1.63×10^{9}	0.021	3.3×10^{-2}	0.19±0.02
Fe, 25°C, pH5, N_2	5.3×10^{-2}*	0.11±0.03*	1.57×10^{-1}	0.26±0.09	2.10×10^{-3}	0.33±0.03	4.1×10^{-17} *	-0.051*	1.30×10^{5}	0.035	3.1×10^{-2}	0.19±0.04
Fe, 25°C, pH6, N_2	8.5×10^{-2}	0.12±0.06*	1.57×10^{-1}	0.26±0.09	9.26×10^{-3}	0.33±0.1	5.1×10^{-9}	-0.058*	1.84×10^{2}	0.023*	1.5×10^{-4}*	0.19±0.03
Fe, 25°C, pH4, CO_2	5.5×10^{-2}	0.13±0.02	1.63×10^{-1}	0.26±0.09	1.29×10^{-3}	0.31±0.1	1.3×10^{-12}	-0.064	1.37×10^{5}	0.028	1.95×10^{-2}	0.24±0.02*
Fe, 25°C, pH5, CO_2	2.5×10^{-1}*	0.12±0.03*	1.63×10^{-1}	0.26±0.09	6.30×10^{-3}	0.32±0.2	1.1×10^{-11} *	-0.075*	1.06×10^{9}*	0.027*	1.9×10^{-2}*	0.28±0.01*
Fe, 25°C, pH6, CO_2	4.1×10^{0}*	0.12±0.02*	1.63×10^{-1}	0.14±0.09*	2.50×10^{1}*	0.35±0.2	5.5×10^{-6} *	-0.076*	1.55×10^{14}*	0.030	1.7×10^{-2}*	0.29±0.01*
Fe, 35°C, pH4, N_2	1.3×10^{-1}	0.12±0.02	1.4×10^{1}	0.11±0.08	9.9×10^{-4}	0.39±0.1	1.2×10^{-20}	-0.029	1.65×10^{9}	0.022	2.56×10^{-2}	0.25±0.02*
Fe, 45°C, pH4, N_2	5.9×10^{-1}*	0.11±0.02*	3.8×10^{2}*	0.11±0.1	8.9×10^{-4}	0.47±0.1	7.6×10^{-14}	-0.056	6.75×10^{3}	0.042	7.2×10^{-1}*	0.25±0.02*
Fe, 35°C, pH4, CO_2	1.4×10^{-1}*	0.12±0.02*	6.5×10^{-1}	0.18±0.1	9.3×10^{-4}	0.44±0.1	1.2×10^{-12}	-0.066	3.34×10^{5}	0.030	2.6×10^{-2}	0.27±0.02*
Fe, 45°C, pH4, CO_2	7.2×10^{-1}*	0.10±0.02*	2.5×10^{0}	0.15±0.09	8.3×10^{-4}	0.49±0.2	1.0×10^{-12} *	-0.059	6.79×10^{1}	0.061	7.5×10^{-1}*	0.24±0.03*
X65, 25°C, pH4, N_2	9.0×10^{-2}*	0.12±0.01	8×10^{-2} *	0.26±0.3*	5.82×10^{-3}	0.17±0.07	1.5×10^{-12}	-0.064	4.74×10^{7}	0.024	7.1×10^{-2}	0.16±0.02*
2% Cr steel, 25°C, pH4, N_2	1.4×10^{-1}*	0.11±0.01	1.7×10^{-1}	0.26±0.3	3.92×10^{-4}	0.39±0.1	6.4×10^{-15}	-0.045	2.32×10^{2}	0.038	3.8×10^{-2}	0.17±0.01*
X65, 25°C, pH4, CO_2	1.4×10^{-1}*	0.11±0.02	9.8×10^{-2} *	0.27±0.7*	5.96×10^{-3}	0.18±0.1	1.1×10^{-10}	-0.104	1.75×10^{9}	0.021	6.7×10^{-2}	0.16±0.02
2% Cr steel, 25°C, pH4, CO_2	2.3×10^{-1}*	0.10±0.03	1.9×10^{-1}	0.25±0.8	5.83×10^{-4}	0.34±0.2	2.6×10^{-11}	-0.076	2.64×10^{3}	0.037	6.2×10^{-2}	0.18±0.01*

Verification of the Proposed Approach & Model

To validate the introduced approach and the model developed for reproducing the anodic dissolution, Figure 7 compares the modeled sweeps with the experimental results. The grey curves represent the experimental data, and the black dashed lines show the model. There is good consistency between the experiment and the modeled sweeps in all three regions of active, transition, and pre-passivation for different experimental conditions. This validates the accuracy of the introduced methodology for calculating the kinetic parameters and subsequently modeling the sweeps.

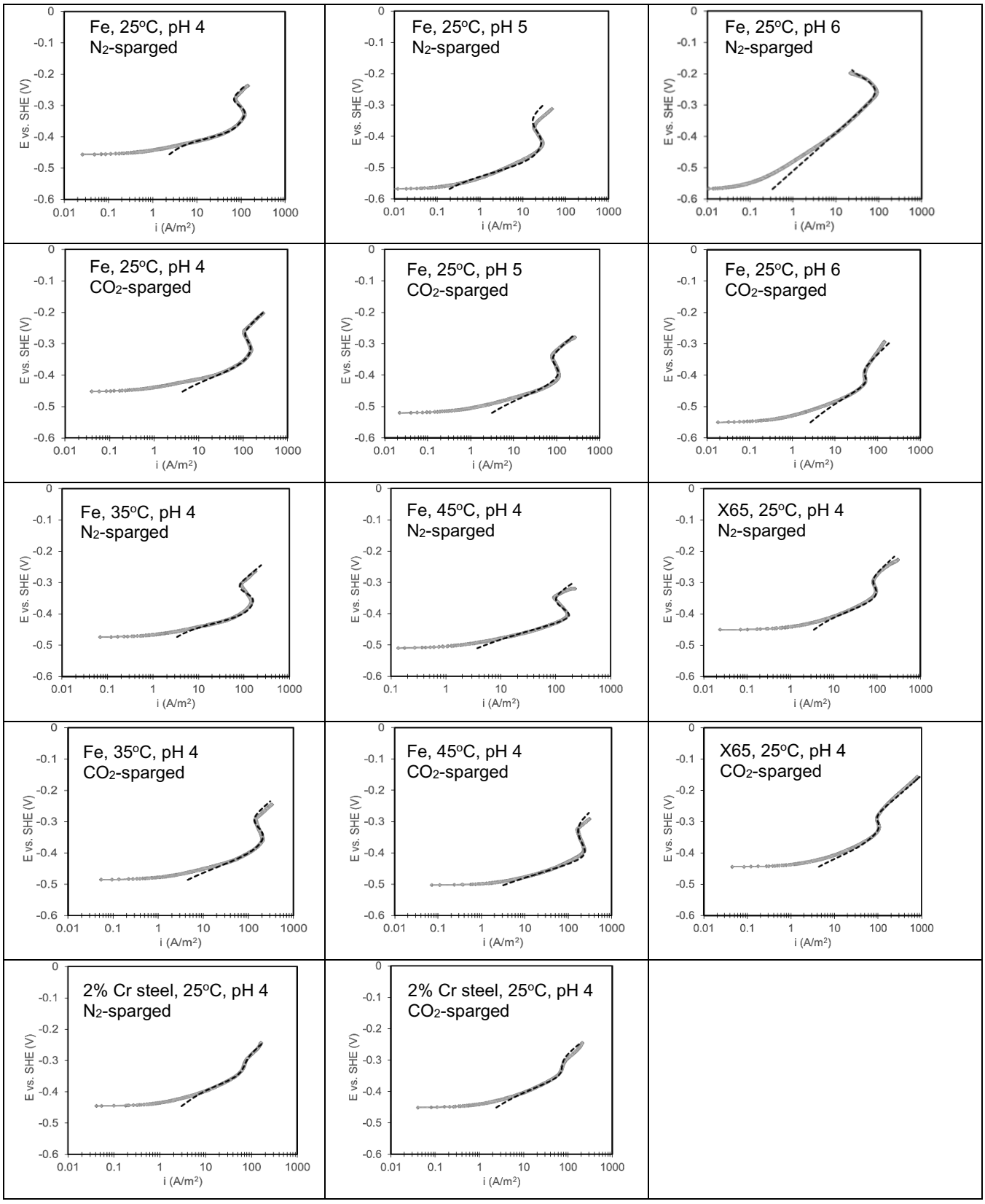

Figure 7. Comparison of the model vs. experiments for different experimental conditions.

The mismatch at lower potentials is because the cathodic reactions were not included in the model. It can be seen from the data in Table 2 that as pH changed or when CO_2 was introduced, the change of the kinetic parameters related to two steps (i.e., 1 and 3) was more significant than other elementary steps. In addition, as the temperature increased the increase of k_2 and k_4 was more noticeable than in other elementary steps. Comparing the data listed in Table 2 also indicates that the steel type impacts the catalytic pathway by mainly affecting step 3 (in both forward and backward directions). The exact correlation between k_i and environmental factors will be discussed qualitatively and quantitatively in greater detail in our next paper.

CONCLUSIONS

A novel approach was established based on transient analysis, to obtain a set of kinetic constants during iron anodic dissolution. Applying these parameters to the most up-to-date theory presented herein, the experimental anodic sweeps were successfully modeled over a wide range of experimental conditions. This research can serve as a base for future studies about the exact impact of environmental factors such as pH, CO_2 presence, temperature, anions, steel type, etc. on the mechanism of steady-state dissolution of iron.

ACKNOWLEDGMENTS

The authors would like to thank the following companies for their financial support:
Ansys, Baker Hughes, Chevron Energy Technology, Clariant Corporation, ConocoPhillips, ExxonMobil, M-I SWACO (Schlumberger), Multi-Chem (Halliburton), Occidental Oil Company, Pertamina, Saudi Aramco, Shell Global Solutions and TotalEnergies.

References

1. K.E. Heusler, Encyclopedia of Electrochemistry of the Elements vol. 9, Marcel Dekker, New York, 1982.
2. J.O. Bockris, D. Drazic, A.R. Despic, “The Electrode kinetics of the deposition and dissolution of iron”, Electrochimica Acta Vol. 4 (1961) pp. 325–361.
3. A.A.E. Miligy, D. Geana, W.J. Lorenz, “A theoretical treatment of the kinetics of iron dissolution and passivation”, Electrochimica Acta 20 (1975) pp. 273-281.
4. M. Keddam, O.R. Mattos, H. Takenouti, “Reaction model for iron dissolution studied by electrode impedance”, J. Electrochem. Soc. 128 (1981) pp. 257-266.
5. M. Keddam, O.R. Mattox, H. Takenouti, “Reaction model for iron dissolution studied by electrode impedance. II. Determination of the reaction model”, J. Electrochem. Soc. 128 (1981) pp. 266-274.
6. M. Keddam, O.R. Mattos, H. Takenouti, “Mechanism of anodic dissolution of iron-chromium alloys investigated by electrode impedance–I. Experimental results and reaction model”, Electrochimica Acta 31 (1986) pp. 1147-1158.
7. M. Keddam, O.R. Mattos, H. Takenouti, “Mechanism of anodic dissolution of iron-chromium alloys investigated by electrode impedance–II. Elaboration of the reaction model”, Electrochimica Acta 31 (1986) pp. 1159-1165.
8. M. Bagheri Hariri, B. Brown, S. Nesic, “Revisiting the anodic dissolution of pure iron in strong acid: replication of Bockris’ estimation of Butler-Volmer”, AMPP Annual Conference + Expo, 2022; Paper No. 17681, San Antonio, Texas, USA.